Constraints on conformal ultralight dark matter couplings from the European Pulsar Timing Array

Clemente Smarra[1,2,*] Adrien Kuntz[1,2,†] Enrico Barausse[1,2] Boris Goncharov[3,4,5,6] Diana López Nacir[7,8]
Diego Blas[9,10] Lijing Shao[11,12] J. Antoniadis[13,14] D. J. Champion[14] I. Cognard[15,16] L. Guillemot[15,16] H. Hu[14]
M. Keith[17] M. Kramer[14,17] K. Liu[14,18] D. Perrodin[19] S. A. Sanidas[17] and G. Theureau[15,16,20]

[1]*SISSA, Via Bonomea 265, 34136 Trieste, Italy, and INFN Sezione di Trieste,*
Galleria Padriciano, 99, 34149 Trieste, Italy
[2]*IFPU—Institute for Fundamental Physics of the Universe, Via Beirut 2, 34014 Trieste, Italy*
[3]*Gran Sasso Science Institute (GSSI), I-67100 L'Aquila, Italy*
[4]*INFN, Laboratori Nazionali del Gran Sasso, I-67100 Assergi, Italy*
[5]*Max Planck Institute for Gravitational Physics (Albert Einstein Institute), D-30167 Hannover, Germany*
[6]*Leibniz Universität Hannover, D-30167 Hannover, Germany*
[7]*Universidad de Buenos Aires, Facultad de Ciencias Exactas y Naturales,*
Departamento de Física, Buenos Aires, Argentina
[8]*CONICET—Universidad de Buenos Aires, Instituto de Física de Buenos Aires (IFIBA), Buenos Aires, Argentina*
[9]*Institut de Fisica d'Altes Energies (IFAE), The Barcelona Institute of Science and Technology,*
Campus UAB, 08193 Bellaterra (Barcelona), Spain
[10]*Institució Catalana de Recerca i Estudis Avançats (ICREA), Passeig Lluís Companys 23, 08010 Barcelona, Spain*
[11]*Kavli Institute for Astronomy and Astrophysics, Peking University, Beijing 100871, China*
[12]*National Astronomical Observatories, Chinese Academy of Sciences, Beijing 100012, China*
[13]*FORTH Institute of Astrophysics, Nikolaou Plastira 100, 70013, Heraklion, Greece*
[14]*Max-Planck-Institut für Radioastronomie, Auf dem Hügel 69, D-53121 Bonn, Germany*
[15]*Laboratoire de Physique et Chimie de l'Environnement et de l'Espace,*
Université d'Orléans/CNRS, 45071 Orléans Cedex 02, France
[16]*Observatoire Radioastronomique de Nançay, Observatoire de Paris,*
Université PSL, Université d'Orléans, CNRS, 18330 Nançay, France
[17]*Jodrell Bank Centre for Astrophysics, Department of Physics and Astronomy, University of Manchester,*
Manchester M13 9PL, United Kingdom
[18]*Shanghai Astronomical Observatory, Chinese Academy of Sciences, 80 Nandan Road, Shanghai 200030, China*
[19]*INAF—Osservatorio Astronomico di Cagliari, Via della Scienza 5, 09047 Selargius (CA), Italy*
[20]*Laboratoire Univers et Théories LUTh, Observatoire de Paris, Université PSL,*
CNRS, Université de Paris, 92190 Meudon, France

Millisecond pulsars are extremely precise celestial clocks: as they rotate, the beamed radio waves emitted along the axis of their magnetic field can be detected with radio telescopes, which allows for tracking subtle changes in the pulsars' rotation periods. A possible effect on the period of a pulsar is given by a potential coupling to dark matter, in cases where it is modeled with an "ultralight" scalar field. In this paper, we consider a universal conformal coupling of the dark matter scalar to gravity, which in turn mediates an effective coupling between pulsars and dark matter. If the dark matter scalar field is changing in time, as expected in the Milky Way, this effective coupling produces a periodic modulation of the pulsar rotational frequency. By studying the time series of observed radio pulses collected by the European Pulsar Timing Array experiment, we present constraints on the coupling of dark matter, improving on existing bounds. These bounds can also be regarded as constraints on the parameters of scalar-tensor theories of the Fierz-Jordan-Brans-Dicke and Damour-Esposito-Farèse types in the presence of a (light) mass potential term.

I. INTRODUCTION

Elucidating the nature of dark matter (DM) remains as one of the most pressing questions of modern physics. The widely accepted cold dark matter (CDM) paradigm successfully explains numerous aspects of the Universe's

*Contact author: csmarra@sissa.it
†Contact author: akuntz@sissa.it

043033-1

large-scale structure but encounters difficulties in predicting some observations on scales smaller than approximately a kiloparsec (~kpc). Notably, observations indicate a flat density profile in the inner regions of galaxies, contradicting the pure CDM prediction of a steep power-law-like behavior (*cusp-core problem*) [1–3]. Additionally, known challenges arise from the mismatch between the observed and expected number of satellites of the Milky Way (MW) (*missing satellite problem*) [4,5], and simulations based on ΛCDM theory suggest that the most massive subhaloes of the MW would be too dense not to host bright satellites (*too-big-to-fail problem*) [6]. Although these issues may be mitigated by considering baryonic feedback mechanisms, such as supernova feedback [7–12], another possibility is to assume that DM is an ultralight scalar field (with mass $m \sim 10^{-22}$ eV) with negligible self-interactions [13,14]. In this scenario, the de Broglie wavelength of the scalar field in galaxies can reach ~kpc, suppressing power on smaller scales while retaining all the successes of CDM at large scales. Furthermore, the presence of ultralight scalars is also motivated from a theoretical standpoint by string theory [15–17]. In this context, the mass range can be much broader, which motivates considering very light bosons in a large span of ultralight masses (including, but not restricted to, $m \sim 10^{-22}$ eV) as natural candidates for theories beyond the Standard Model.

Numerous studies have been conducted to investigate the existence of ultralight DM (ULDM). Among them, the integrated Sachs-Wolfe effect on the cosmic microwave background (CMB) anisotropies excludes masses $m \lesssim 10^{-24}$ eV [18]. Lyman-α observations strongly suggest a lower limit of $m \gtrsim 10^{-21}$ eV for ultralight candidates accounting for more than $\sim 30\%$ of the DM [19–23]. However, the susceptibility of non-CMB constraints to uncertainties in the modeling of small-scale structure properties [24,25] emphasizes the importance of complementary and independent investigations. In this context, the rotation curves of well-resolved nearby galaxies also disfavor masses $m \lesssim 10^{-21}$ eV [26]. In addition, measurements of stellar orbit kinematics in ultrafaint dwarf (UFD) galaxies may potentially constrain the scalar field mass to be $m \gtrsim 10^{-19}$ eV, although this remains a topic of ongoing debate [27,28]. Dwarf galaxies can also be used to set robust bounds $m \gtrsim 10^{-22}$ eV [14,29]. Given these observations, the current lore is to consider that ULDM of mass below $m \sim 10^{-22}$ eV cannot constitute 100% of the dark matter, but masses below these bounds are certainly possible if they constitute a fraction of the dark matter—see Ref. [30]. This possibility is natural in the case of the axiverse, where several ULDM candidates coexist at low masses [31], and also for ultralow-mass particles that may be cosmologically produced to significant values—see, e.g., Ref. [32].

A completely independent method to probe these small masses was suggested in Ref. [33], where it was pointed out that the oscillating *gravitational potential* induced by the presence of ULDM influences the light travel time of radio signals emitted by pulsars. Pulsar Timing Array (PTA) experiments [34–39] rely on the exquisite predictability of the millisecond pulsar (MSP) spin period's behavior. Each time a MSP magnetic field axis points toward Earth, radio waves are observed by radio telescopes. After measuring and modeling consecutive pulses in decade-long observational campaigns, PTAs search for signals of physical effects that affect all of the observed pulsars, including the ULDM signal. Based on this principle, previous PTA searches have established 95% upper limits on the local energy density of ULDM, reaching $\rho \lesssim 0.15$ GeV/cm^3 in the mass range $10^{-24.0}$ eV $\lesssim m \lesssim 10^{-23.7}$ eV [40,41].

The ideas of Ref. [33] rely on the universal gravitational coupling of DM to ordinary matter. However, ULDM may also be coupled to the Standard Model fields [42,43]. Indeed, a natural possibility that respects the weak equivalence principle is that ULDM may be universally (conformally) coupled to gravity, or (equivalently, in the Einstein frame) to the Standard Model. This universal coupling, together with the oscillations of the scalar field in the MW, would give rise to periodic orbital perturbations in binary systems, which allows us to place constraints on the model [44–46]. In this context, ULDM may be regarded as a scalar-tensor theory of the Fierz-Jordan-Brans-Dicke [47–50] or Damour-Esposito-Farèse type [51,52], in the presence of a (light) mass potential term [53]. As a result of the strong gravitational fields active inside neutron stars, the conformal coupling to gravity gives rise to an effective (gravity-mediated) interaction between neutron stars (and thus pulsars) and the scalar ULDM field [51,54–58]. This effect, known as the Nordtvedt effect [54], violates the strong equivalence principle, and it has long been constrained with binary pulsar data [59–66].

In a recent companion paper [67], following former studies [56,58,68], two of us computed the effect of this effective interaction on the rotational period of an *isolated* pulsar. More specifically, Ref. [67] found that the effective coupling between ULDM and pulsars produces a change in the moment of inertia (and therefore in the rotational period) of the pulsar. This change is proportional to the rate of change (in time) of the scalar field, which—as mentioned above—is expected to oscillate in the MW. Deriving precise constraints from current observations on the conformal ULDM coupling based on this effect is the main objective of this work.

This work is structured as follows: In Sec. II, we define the Lagrangian of our theory, and we briefly review some general features of ULDM relevant to our analysis. Section III will be devoted to a detailed description of the dataset and the procedure used to carry out the analysis. Finally, in Sec. IV, we will show how a nonminimally coupled ULDM candidate affects the spin frequency of MSPs. We constrain the coupling strength, resulting in

bounds which are several orders of magnitude better than what has been obtained from Cassini tests of general relativity [44,69], or from the pulsar in a triple stellar system [62–64] in the mass region to which PTAs are sensitive. Our conclusions are presented in Sec. V. The Appendix is devoted to technical details and plots.

II. CONFORMALLY COUPLED ULTRALIGHT DARK MATTER

Light scalar and pseudoscalar fields emerge naturally from string theory and from theories with pseudo-Goldstone bosons (as the axions introduced to tackle the strong CP problem) [31,70,71]. These fields are, in principle, coupled to Standard Model fields. Hence, it is natural to consider *nonminimally coupled* scenarios when exploring their phenomenology. In this work, we consider a scalar field ϕ with mass m. The action for this field in the Einstein frame is given by[1]

$$S = M_{\rm P}^2 \int {\rm d}^4x \sqrt{-g} \left[\frac{R}{2} - g^{\mu\nu}\partial_\mu\phi\partial_\nu\phi + m^2\phi^2 \right] + S_m[\psi_m, \tilde{g}_{\mu\nu}],   \tag{1}$$

where $M_{\rm P}$ is the Planck mass, and the matter action S_m includes a universal *conformal* coupling of the scalar field to the matter content ψ_m through the (Jordan) effective metric $\tilde{g}_{\mu\nu} = \mathcal{A}^2(\phi)g_{\mu\nu}$, normalized such that $\mathcal{A}^2(0) = 1$. Note that when reexpressed in the Jordan frame, this direct coupling to matter disappears and is replaced by a conformal coupling to gravity (i.e., to the Ricci scalar). In other words, this model satisfies the weak equivalence principle. In particular, the free-fall motion of nongravitating objects is universal (i.e., independent of the body composition) [72]. However, in strongly gravitating objects (such as neutron stars), there appears an effective (tensor-mediated) coupling between matter and the scalar field.

As a first model, we consider the Fierz-Jordan-Brans-Dicke (FJBD) theory [47–50], in which the conformal coupling is linear:

$$\mathcal{A}(\phi) = e^{\alpha\phi} \sim 1 + \alpha\phi.   \tag{2}$$

The constant *scalar coupling* α is constrained by several observations, notably by the Cassini mission to the level of $\alpha^2 \lesssim 10^{-5}$ [69] and by the triple system PSR J0337 + 1715 to the level of $\alpha^2 \lesssim 4 \times 10^{-6}$ [64]. A simple way to evade this constraint is to consider masses generating a Yukawa suppression at scales of the order of the typical distances probed by these systems [53]. Since our focus is on the PTA, and hence on DM masses with Compton wavelength

larger than $\sim 10^3$ AU, this constraint applies to the models we explore.[2]

As a second model, we also consider the Damour-Esposito-Farèse (DEF) gravity theory [51,52], where the conformal coupling is quadratic:

$$\mathcal{A}(\phi) = e^{\beta\phi^2/2}.   \tag{3}$$

Notice that we have chosen to set the linear coupling of the field in $\mathcal{A}(\phi)$ to zero, so that the FJBD theory cannot be recovered as a special case of DEF gravity; rather, the two theories are part of a more general theory, where both linear and quadratic couplings are nonzero. The absence of significant deviations from the general relativity (GR) predictions in binary pulsar data requires $\beta \gtrsim -4.3$ [depending on the exact equation of state (EOS) for the neutron star model] in order to avoid nonperturbative spontaneous scalarization phenomena [52,73], while the value ϕ_0 of the scalar field on cosmological scales is constrained by the Cassini (pulsar in a triple stellar system) bound to the level $(\beta\phi_0)^2 \lesssim 10^{-5}$ and by the pulsar in a triple stellar system to $(\beta\phi_0)^2 \lesssim 4 \times 10^{-6}$.

The energy-momentum tensor of the scalar field sourcing the metric $g_{\mu\nu}$ on cosmological scales follows, in the Einstein frame, from Eq. (1):

$$T_{\mu\nu} = M_{\rm P}^2 \left[2\partial_\mu\phi\partial_\nu\phi - g_{\mu\nu} \left((\partial\phi)^2 - m^2\phi^2 \right) \right].   \tag{4}$$

In the Jordan frame $\tilde{T}_{\mu\nu} = \mathcal{A}^{-2}(\phi)T_{\mu\nu}$, it reduces to

$$\tilde{T}_{\mu\nu} = \mathcal{A}^{-2}(\phi)T_{\mu\nu} \simeq \left(1 - 2\alpha(\phi) \right) T_{\mu\nu},   \tag{5}$$

where the effective scalar coupling is[3] $\alpha(\phi) = {\rm d}\log\mathcal{A}/{\rm d}\phi$, and we work in the limit $\alpha(\phi) \ll 1$. The mass of the scalar field can be as small as $m \sim 10^{-22}$ eV and still be a viable very light candidate for CDM. We will refer to models of masses not far from this limit as ULDM. In these models, the distances between particles are much smaller than the corresponding de Broglie wavelength, which implies that they can be treated as a classical superposition of free waves with dynamical properties generated by galactic dynamics. For the MW, this superposition has a very small dispersion velocity ($\sigma_\phi \sim 10^{-3}$), and therefore the ULDM field can be described as a standing wave[4]:

---

[1]Note that our scalar field ϕ is not canonically normalized, but rather appears in the action multiplied by $M_{\rm P}$. This convention makes comparisons with gravitational phenomena more straightforward.

[2]The center of mass of the inner binary in the triple system PSR J0337 + 1715 completes a rotation around the center of mass of the entire system in about 327 days [64], which corresponds to a distance of $\sim$0.9 AU.

[3]In order to avoid confusion, we stress that $\alpha(\phi)$ is generally different from α, but reduces to it in FJBD theory. Binary pulsars have constrained $|\alpha(\phi)|$ to be $\lesssim 10^{-2}$ for neutron stars [66].

[4]Close to the Galactic Center, the distribution may condense into a different configuration known as a "soliton" or "Bose star" [24]. We will not deal with this situation, since the pulsars used by the PTA are far from the Galactic Center.

$$\phi(\boldsymbol{x}, t) = A(\boldsymbol{x}) \cos\big(mt + \theta(\boldsymbol{x})\big), \qquad (6)$$

with $A(\boldsymbol{x})$ determined by[5]

$$\tilde{\rho}_\phi \approx \rho_\phi = m^2 M_{\rm P}^2 A(\boldsymbol{x})^2 = \rho \hat{\phi}(\boldsymbol{x})^2, \qquad (7)$$

where we have used Eq. (5) to relate the stress-energy-momentum tensor in the Einstein frame to the one in the Jordan frame, and we have neglected the terms $\sim(\partial_i\phi)^2$ which are suppressed by v_ϕ^2. Here, ρ is the average density of the scalar field, and $\hat{\phi}(\boldsymbol{x})$ is a *stochastic* parameter extracted from the Rayleigh distribution $[P(\hat{\phi}^2) = e^{-\hat{\phi}^2}]$ [74]. This parametrization takes into account the fact that the ULDM configurations are built by the superposition of several waves of random phases that interfere. For the average density, we take $\rho = \rho_{\rm DM} = 0.4$ GeV/cm^3 as a benchmark value for the *average* DM density expected at the Sun's position in the Milky Way [75]. As commented on in the Introduction, masses $m \lesssim 10^{-22}$ eV are strongly disfavored to constitute all the dark matter in our Galaxy. As a result, for these masses, one needs to focus on scenarios where ULDM is a fraction $f_{\rm DM} \equiv \rho/\rho_{\rm DM} < 1$. The factor $\hat{\phi}$ appears from the interference caused by the wavelike nature of the scalar field. It reproduces the expected random local value from the superposition of the waves, and it makes the scalar field density $\tilde{\rho}_\phi$ approach ρ when averaging over timescales longer than the ULDM *coherence time*:

$$\tau_c \sim \frac{2}{mv^2} = 2 \times 10^5 \text{ yr}\left(\frac{10^{-22} \text{ eV}}{m}\right), \qquad (8)$$

or, equivalently, on a length scale larger than the ULDM *coherence length*:

$$l_c \sim \frac{1}{mv} \sim v \cdot \tau_c \sim 0.4 \text{ kpc}\left(\frac{10^{-22} \text{ eV}}{m}\right). \qquad (9)$$

We have conveniently normalized the mass to values relevant to PTA observations. In the Jordan frame, an oscillating scalar field, such as the one presented in Eq. (6), induces a temporal variation of Newton's constant. Its measured value is [51]

$$G = (8\pi M_{\rm P}^2)^{-1}\mathcal{A}^2(\phi)(1 + \alpha^2(\phi)), \qquad (10)$$

where $\alpha(\phi) = \mathcal{A}'(\phi)/\mathcal{A}(\phi)$. In order to use this property of scalar-tensor theories, we follow Ref. [67] and neglect the scalar field mass on the typical length scale of a pulsar, a valid approximation given our mass range for ULDM. In turn, a variation of the local gravitational constant modifies

the gravitational mass and the radius of the neutron star [51]. This dependence is encoded in the *sensitivities*, which represent the rate of change of these parameters with respect to changes in the scalar field [72].

To explore this effect, one can recall that the conservation of angular momentum J relates the changes in the moment of inertia I of the neutron star (depending on the local value of G) to the observed pulse frequency $\Omega_{\rm obs}$ through the relation $J = I\Omega_{\rm obs}$. Particular attention has to be paid to the frame used for the definition of the angular momentum J, as the latter is only conserved in the Einstein frame (see Ref. [67] for more details). We use the code presented in Ref. [67] to compute the angular momentum sensitivity, defined by

$$s_I = -\frac{1}{2\alpha(\phi)}\frac{\rm d\ln I}{\rm d\phi}\bigg|_{N,J} = \frac{1}{2\alpha(\phi)}\frac{\rm d\ln \Omega_{\rm obs}}{\rm d\phi}\bigg|_{N,J}, \quad (11)$$

where the pulsar's baryon number N and the Einstein-frame angular momentum J are kept constant. With this sensitivity at hand, a change in the scalar field value can be directly related to a change in the frequency of the pulsar, and consequently, to a change in the pulsar's pulse time of arrival (TOA). We will use this fact in Sec. IV to constrain ULDM models.

III. DATASET AND METHODOLOGY

In this work, we analyze the second data release (DR2) [76] of the European Pulsar Timing Array (EPTA) Collaboration [37,77]. In particular, we use the EPTA-DR2Full dataset,[6] consisting of 24.7 years of collection of the TOAs of radio pulses of 25 ms pulsars, surveyed with an approximately biweekly cadence[7] and observed by five telescopes located in France, Germany, Italy, the Netherlands, and the United Kingdom. The relation between the time of emission of a radio pulse and its TOA at the Solar System barycenter (SSB) is encoded in a pulsar-specific *timing model* [78], which takes into account the pulsar spindown, its position and proper motion, the motion around a binary companion, etc. Any deviations between the predicted TOAs and the actual measurements, referred to as *timing residuals*, may include contributions from various sources of noise, including stochastic dispersion measure fluctuations and irregularities in pulsar rotation [79,80]. However, these residuals might also be indicative of processes of astrophysical significance, cf. the recent evidence of a stochastic gravitational wave background (SGWB) in the data of various PTA experiments [81–84].

---

[5]Notice that, as compared to field theory conventions, there are factors of 2 in difference, arising from the noncanonical normalization of the scalar field in Eq. (1).

[6]The dataset can be found at https://gitlab.in2p3.fr/epta/epta-dr2.

[7]The cadence is nonuniform. EPTA combines observations from several telescopes, so sometimes the EPTA-wide cadence can be much shorter.

Because the EPTA-DR2Full dataset does not yield a strong evidence in favor of the hallmark Hellings-Downs (HD) [85] interpulsar correlation (in contrast to the 10.3 yr dataset [76,80,86,87]), we only account for possible contributions from the SGWB via a PTA-wide spatially uncorrelated but temporally correlated noise term, characterized by an amplitude A_{GWB} and a spectral index γ_{GWB} (see Table I for more details). Such a signal appears as a precursor to the SGWB [88–90], because of the stronger autocorrelation of the Hellings-Downs process.

We utilize Bayesian inference to detect the ULDM-induced *deterministic*[8] signal, while simultaneously marginalizing over timing model parameters [76] and accounting for all known sources of noise in the data [80]. Given the model parameters θ, the likelihood function for the timing residuals, denoted as $\mathcal{L}(\delta t|\theta)$, is represented as [91–95]:

$$\ln \mathcal{L}(\delta t|\theta) \propto -\frac{1}{2}(\delta t - \mu)^{\mathrm{T}} C^{-1}(\delta t - \mu). \quad (12)$$

In this time-domain Gaussian likelihood, δt is a vector with dimension corresponding to the number of observations. The deterministic ULDM contribution, which we derive below in Eqs. (19) and (23), is taken into account in μ, which includes contributions from both the timing model and noise processes, as analyzed in Ref. [80]. Temporally uncorrelated "white" noise and other sources of uncertainty in TOA measurements are factored into the diagonal components of the covariance matrix C. Off-diagonal elements of the matrix C could, in principle, contain contributions from temporally correlated "red" noise; yet they are more commonly incorporated into μ for computational efficiency, following the approach described in Refs. [92,93]. The priors $\pi(\theta)$ of the parameters used for the search are described in Table I. Parameter estimations are carried out by evaluating posterior distributions, denoted as $\mathcal{P}(\theta|\delta t) \propto \mathcal{L}(\delta t|\theta)\pi(\theta)$, produced with the Parallel-Tempering Markov-Chain Monte-Carlo sampler [96] implemented in ENTERPRISE [94] and ENTERPRISE_EXTENSIONS [95], using the PTArcade [97,98] wrapper and adapting it to the EPTA dataset.

In this work, we consider the effect of the scalar field on the TOAs, and we constrain the conformal coupling by looking at its effect on the timing residuals. Since the duration $T_{\mathrm{obs}} = 24.7$ yr of the EPTA-DR2Full dataset is much shorter than the coherence time in Eq. (8) for the ULDM considered here, different coherence patches with characteristic dimension l_c will have different ρ_ϕ values. However, notice that if m is sufficiently small that $l_c > R$, where R is the characteristic radius probed by Galactic rotation curves, we are really observing one single patch of ULDM. We refer to this case as the *correlated* scenario.

Based on these premises, we thus distinguish three different regimes [40], according to the interplay between the mass of the ULDM candidate and the typical interpulsar separation. In the *uncorrelated* regime, each of the pulsars timed by the EPTA resides in a different coherent patch. Therefore, each pulsar is characterized by its own $\hat{\phi}(\boldsymbol{x})$ parameter. As the average interpulsar distance is $\mathcal{O}(\mathrm{kpc})$, the *uncorrelated* approximation holds for ULDM masses $m \gtrsim 5 \times 10^{-23}$ eV. For masses $m \lesssim 2 \times 10^{-24}$ eV (*correlated* scenario), the coherence length described by Eq. (9) encompasses the inner galactocentric ~ 20 kpc, which is the benchmark area examined by the most accurate measurements of MW rotation curves [75], from which the local DM abundance is inferred. Therefore, as the kinematic tests of the DM halo explore the same coherence patch that hosts all the EPTA pulsars, we can safely absorb the *common* parameter $\hat{\phi}(\boldsymbol{x})$ into the measured value of the local ULDM abundance. Equation (6) then reads

$$\phi(\boldsymbol{x}, t) = \frac{\sqrt{\rho}}{m M_{\mathrm{P}}} \cos(mt + \theta(\boldsymbol{x})), \quad (13)$$

with ρ representing the value of the scalar field density ρ_ϕ in our Galaxy. Finally, for masses 2×10^{-24} eV $\lesssim m \lesssim 5 \times 10^{-23}$ eV, one ULDM coherence patch can encompass all pulsars, but it does not reach the typical radius explored by rotation curves. In this *pulsar-correlated* scenario, the stochastic parameter $\hat{\phi}(\boldsymbol{x})$ is common across all the pulsars. However, estimates of DM density derived from rotation curves average over different coherence patches. Hence, we maintain $\hat{\phi}(\boldsymbol{x})$ as an independent parameter and marginalize over it, so that the constraints on ρ derived from the following analysis can be compared to the density estimated through rotation curves. Regardless of the scenario, we always draw one phase parameter $\theta(\boldsymbol{x})$ per pulsar. This phase encodes the uncertainty on current pulsar distance measurements [40,99,100] [see below Eq. (16) in Sec. IV for more details].

We focus on the ULDM mass range $m \in [10^{-24}$ eV, 10^{-21} eV], since this is the interval where PTA constraints are the most compelling. Notice that the low-mass end corresponds to a frequency of $f_{\mathrm{low}} \sim 2.4 \times 10^{-10}$ Hz, which is far below the inverse of the EPTA-DR2Full observation length $f_{\mathrm{obs}} = 1/T_{\mathrm{obs}} \sim 1.3$ nHz. In this regime, the ULDM-induced signal [see Eq. (19) later] can still be expanded in powers of (mt) [42]. The first terms in the expansion are degenerate, with the simultaneous fitting of pulsar spin frequency derivatives [101–103]; therefore, the lowest-order term that PTAs are sensitive to is $(mt)^3$. Although this introduces a sensitivity loss—which is also confirmed, e.g., by Fig. 2—the ULDM-induced signal amplitude is inversely proportional to the particle mass [see Eqs. (18) and (19)]. Therefore, we can still provide significant bounds at $f \lesssim 1/T_{\mathrm{obs}}$ [104]. The

---

[8]The signal induced by ULDM is deterministic, as opposed to the stochastic nature of, e.g., the common red noise process describing the SGWB.

upper end of the ULDM mass range instead corresponds to $f_{\rm up} \sim 2.4 \times 10^{-7}$ Hz, which is somewhat lower than the observational cadence of $f \sim 1/2$ weeks $\sim 8.3 \times 10^{-7}$ Hz, after which the PTA data are not sensitive. Finding no evidence for a signal in the examined mass range, we present 95% upper limits in the following sections.

IV. RESULTS

In this section, we apply the theoretical framework laid down in Sec. II to constrain the FJBD and the DEF conformal couplings.

A. FJBD conformal coupling

Let us focus on FJBD theory. In this case, by inspecting Eq. (2) and recalling the definition of $\alpha(\phi)$, we find $\alpha(\phi) = \alpha$. Moreover, the numerical analysis carried out in Ref. [67] shows that the angular momentum sensitivity s_I has a very weak dependence on the scalar coupling α that we neglect in this analysis. Depending on the context, we can conveniently write $s_I(\alpha, M)$ as $s_I(M)$ or s_I to avoid cluttering the notation.

For small scalar fluctuations such as the ones considered in this article, it follows from Eq. (11) that

$$\Omega_{\rm obs}(t) = \bar{\Omega}\big(1 + 2\alpha s_I \delta\phi(t)\big)$$
$$= \bar{\Omega}\left(1 + 2\alpha s_I \frac{\sqrt{\rho}}{M_{\rm P} m} \hat{\phi}(\boldsymbol{x}) \cos\big(mt + \theta(\boldsymbol{x})\big)\right), \quad (14)$$

where we use Eq. (6), and we denote the spin frequency of the pulsar *in the absence of* the scalar field by $\bar{\Omega}$. Notice that Eq. (14) describes the correct frequency shift only under the assumption that the oscillating timescale $t_{\rm osc} \sim 1/m$ is much longer than the timescale on which a neutron star adjusts its internal structure ($t_{\rm int}$). This is a reasonable assumption. For instance, the Vela pulsar shows a fast core-crust coupling with a timescale $t_{\rm int} \sim 10$ s [105], which would be larger than $t_{\rm osc}$ only for ULDM masses $m \gtrsim 10^{-16}$ eV, which are not discussed here (see Sec. III).

To find the TOA change induced by the scalar field, we write Eq. (11) as

$$\frac{\delta\Omega_{\rm obs}}{\bar{\Omega}} = 2\alpha s_I \delta\phi = -\frac{\delta P}{\bar{P}}, \quad (15)$$

where $\bar{P}$ is the pulsar period *in the absence of* the scalar field. The total timing residual $\Delta t(t)$ after a time t is the integral of infinitesimal period variations over time:

$$\Delta t(t) = -\int dt \frac{\delta\Omega_{\rm obs}}{\bar{\Omega}}$$
$$= 2\alpha s_I \frac{\sqrt{\rho}}{M_{\rm P} m^2} \hat{\phi}(\boldsymbol{x}) \sin\big(mt + \theta(\boldsymbol{x})\big)\bigg|_{t_{\rm start}-\frac{d}{c}}^{t_{\rm end}-\frac{d}{c}}, \quad (16)$$

where we have highlighted the dependence on the *retarded* time $t_i - d/c$, with $i = {\rm start, end}$, and d referring to the Earth-pulsar distance. As mentioned before, the pulsar distance can be reabsorbed in a redefinition of the phase $\theta(\boldsymbol{x}) \to \theta(\boldsymbol{x}) + md/c$. Present uncertainties on the pulsar distances are $\mathcal{O}(0.1 \div 1)$ kpc [99], implying that this redefinition gives rise to an effective pulsar-dependent random phase. Therefore, as mentioned in Sec. III, we treat $\theta(\boldsymbol{x})$ as a *pulsar-specific* random parameter, and we neglect the distance in the retarded time from now on.

In analogy with the ULDM search results in Ref. [40], where the timing residual for the model considered was written as

$$\delta t_{\rm DM} = \frac{\Psi_{\rm c}}{2m} [\hat{\phi}_{\rm E}^2 \sin(2mt + \theta_{\rm E}) - \hat{\phi}_{\rm P}^2 \sin(2mt + \theta_{\rm P})], \quad (17)$$

with E and P labeling the Earth and the pulsar,[9] respectively, we can define an *effective* amplitude

$$\Psi = 2\alpha \frac{\sqrt{\rho}}{M_{\rm P} m}, \quad (18)$$

such that

$$\Delta t(t) = \frac{\Psi}{m} s_I \hat{\phi}(\boldsymbol{x}) \sin(mt + \theta(\boldsymbol{x}))\bigg|_{t_{\rm start}}^{t_{\rm end}}. \quad (19)$$

This form helps us to understand what a sensible prior on Ψ may be. In fact, noticing that Eqs. (17) and (19) have the same form [differing only for the presence of the Earth term and some $\mathcal{O}(1)$ factors], we can use the same prior for Ψ and Ψ_c: i.e., $\mathrm{Log}_{10} - \mathrm{Uniform}[-20, -12]$. In other words, the similarity between the two equations shows that what we are really testing is whether the PTA data can constrain the presence of a sinusoidal signal.

As previously stated, the sensitivity s_I as a function of the pulsar mass is computed from a fit to the models of Ref. [67]. In particular, we consistently utilize the pulsar *gravitational* mass as a parameter of the fit instead of the *inertial* mass, because the former is the value measured by experiments. We implement the pulsar masses in the analysis in the following way:

(1) If a pulsar mass is determined from other experiments as $M \pm \delta M$, we draw the mass from a normal distribution centered on M, with uncertainty δM and truncated for masses below $M_{\rm min} = 1.1 M_\odot$ and above $M_{\rm max} \sim 2M_\odot$. The precise value of $M_{\rm max}$ depends on the EOS considered (see the Appendix for more details).

(2) If we have no determination of the pulsar mass, we draw it from a uniform distribution (e.g.,

___
[9]The stochastic parameter $\hat{\phi}_{\rm P}$ corresponds to $\hat{\phi}$ in our notation.

$M \in [1.1 M_\odot, 2.2 M_\odot]$ for the AP4 model; see the Appendix for more details).

At this point, it is worth obtaining some analytical understanding of the results that we expect for α. In particular, in writing the residual induced by an ULDM candidate of mass m as $\Delta t(m)$, we notice that

$$\Delta t(m) \sim \delta t_{\mathrm{DM}}\left(\frac{m}{2}\right) \to \Psi \sim \Psi_c\left(\frac{m}{2}\right), \qquad (20)$$

which, through Eq. (18), yields

$$\alpha \sim \frac{m M_{\mathrm{P}}}{\sqrt{\rho}} \Psi_c\left(\frac{m}{2}\right). \qquad (21)$$

By substituting the upper limits for Ψ_c found in Fig. 1 of Ref. [40], Eq. (21) gives us an approximate estimate of the upper limits that we expect to find. Figure 1 shows the comparison between the *correlated limit* and its theoretical prediction based on Eq. (21), assuming for reference $\rho = \rho_{\mathrm{DM}} = 0.4 \text{ GeV/cm}^3$. As can be seen, our analytical prediction captures the scaling and the overall shape of the constraints, but there are deviations caused by the intrinsic difference between the signals in Eqs. (17) and (19) (for example, the fact that, in our scenario, the timing residual depends on the mass of the pulsar through the sensitivity).

Constraints on $\log_{10} \alpha$ vs ULDM mass
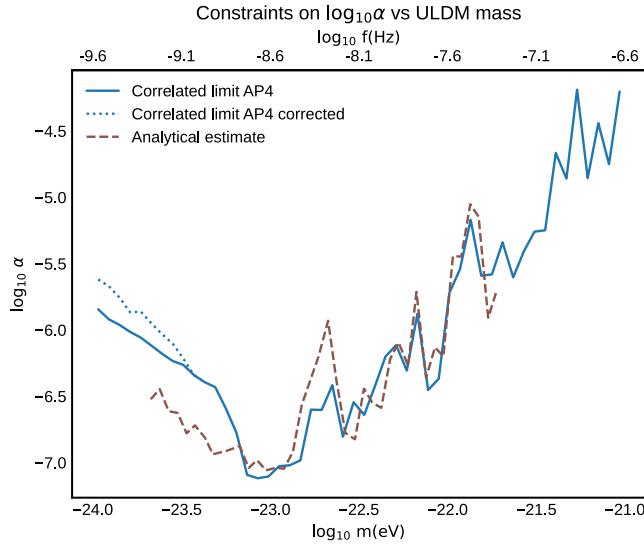
FIG. 1.   Upper limits on $\log_{10} \alpha$ at 95% credibility compared to the analytical estimate described by Eq. (21), for the AP4 EOS. The solid line shows the upper limits on $\log_{10} \alpha$ for the *correlated* analysis, assuming that the background DM density is $\rho_{\mathrm{DM}} = 0.4 \text{ GeV/cm}^3$, while the brown dashed line displays the expected behavior described by Eq. (21). The dotted line shows the degradation of the bounds when choosing $\rho = \min(\bar{\rho}, \rho_{\mathrm{DM}})$, optimistically setting $\bar{\rho}$ to the upper bounds presented in Ref. [40]. Smaller ρ values yield a stronger degradation of the limits.

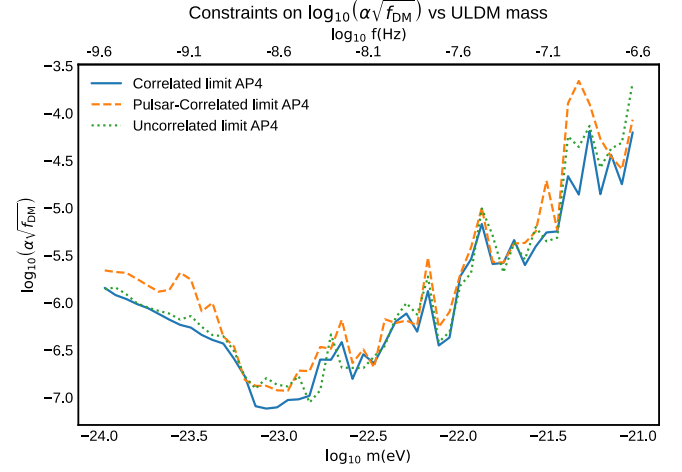Constraints on $\log_{10}(\alpha\sqrt{f_{\mathrm{DM}}})$ vs ULDM mass

FIG. 2.   Upper limits on $\log_{10}(\alpha\sqrt{f_{\mathrm{DM}}})$ at 95% credibility versus the ULDM mass. We compare results for the *correlated*, *pulsar-correlated*, and *uncorrelated* scenarios using solid, dashed, and dotted lines, respectively. The results are obtained using the AP4 EOS, and the priors on the parameters of the search are presented in Table I. Bounds from the Cassini mission and from the pulsar in a triple stellar system constrain $\alpha^2 \lesssim 10^{-5}$ and $\alpha^2 \lesssim 4 \times 10^{-6}$, respectively.

In the following, we present results in terms of $\alpha\sqrt{f_{\mathrm{DM}}}$ to take into account the relative energy density of this ULDM candidate, f_{DM}. This is indeed the quantity constrained by Eq. (18), and it allows for rapidly obtaining the relevant bound on α once a value for the scalar field density ρ is chosen. Figure 2 displays the upper limits for the *correlated*, *pulsar-correlated*, and *uncorrelated* analyses.

We detect the existence of additional signal power above the common red noise background for masses around $m \sim 10^{-22.7}$ eV and $m \sim 10^{-21.4}$ eV across all the three analyses. The first excess is consistent with what was observed in recent searches [40,43], while the second one is thought to be associated with unmodeled perturbations in the orbital elements of Mercury, whose synodic period matches the detected excess frequency [41]. While both of them could in principle be interpreted as evidence of nonminimally coupled ULDM candidates, the fact that they can be accounted for by different physical models makes us more cautious in drawing definitive conclusions. In order for our results to be consistent, we also need to ensure that the effect that we are constraining is not subdominant with respect to the TOA induced by the purely gravitational effect of the ULDM oscillations [33,40], which we are neglecting in our analysis. To understand the interplay between our analysis and the analysis *à la* Khmelnitsky-Rubakov performed in Ref. [40], it is sufficient to notice that a nonminimally coupled ULDM candidate of mass m described by the FJBD action [Eqs. (1) and (2)] will in general produce both an α-*dependent* residual and a *propagation* residual, described by Eqs. (16) and (17), respectively. While the former has a dependence on the

scalar coupling α and has a characteristic frequency $2\pi f = m$, the latter only depends on the density of the scalar field and has a characteristic frequency $2\pi f = 2m$ [33,40]. Therefore, we only need to be careful selecting a value of ρ which is not already excluded by the analysis *à la* Khmelnitsky-Rubakov when extracting a bound on α. Figure 1 shows the effect of this remark on our bounds when we include the constraints on ρ found in Ref. [40].

Additionally, we notice in passing that the form of the signal in Eq. (19) is similar to Eq. (12) in Ref. [42], where direct couplings between ULDM and ordinary matter were also studied with PTA data, apart from $\mathcal{O}(1)$ numerical factors. Mapping our signal to Eq. (12) in Ref. [42], we find

that the limits obtained here are in general agreement with their analysis. Although the two models induce a similar TOA change, it is important to point out that they are fundamentally different. Indeed, the model presented in Ref. [42] introduces a *direct* and particle-dependent coupling of the scalar to matter, which implies a violation (albeit small) of the weak equivalence principle. Instead, our model relies on a universal conformal coupling of the scalar to gravity, and the weak equivalence principle is satisfied (although the strong equivalence principle is violated).

B. DEF theory

To study the DEF theory (quadratic conformal coupling), we recall that it is characterized by $\alpha(\phi) = \beta\phi$, cf. Eq. (3).
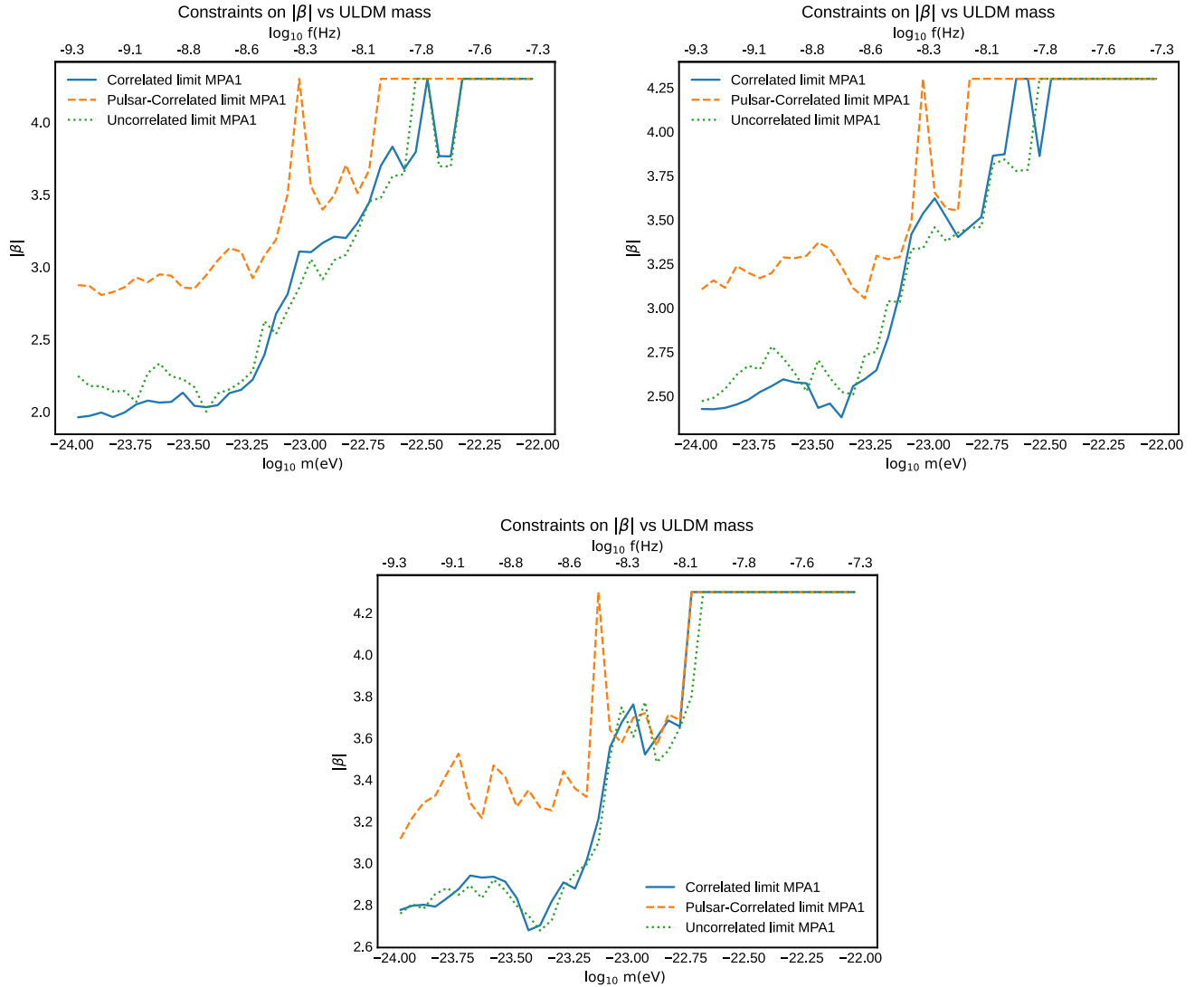
FIG. 3. Upper limits on $|\beta|$ ($\beta < 0$) at 95% credibility versus the ULDM mass. The top-left panel shows the results for $\rho = \rho_{\mathrm{DM}}$, the top-right panel assumes $\rho = 0.5\rho_{\mathrm{DM}}$, and the bottom panel displays the results for $\rho = 0.3\rho_{\mathrm{DM}}$. We compare results for the *correlated, pulsar-correlated*, and *uncorrelated* scenarios in solid, dashed, and dotted lines, respectively. Whenever the bound is prior dominated, the upper limits represent the upper end (in absolute value) of our prior. Priors on the parameters relevant for the search are chosen according to the scheme presented in Table I.
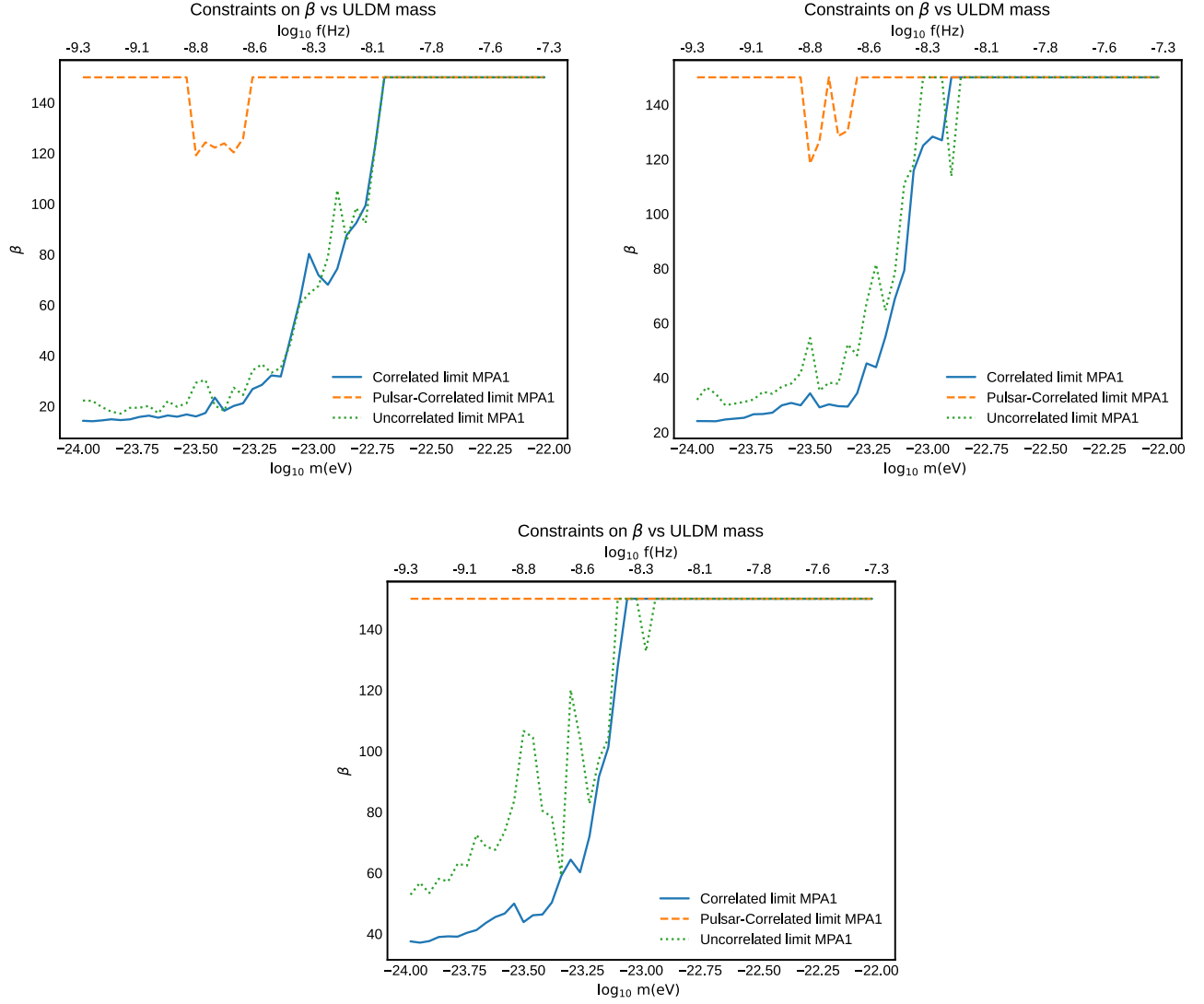
FIG. 4.   Upper limits on β ($\beta > 0$) at 95% credibility versus the ULDM mass. The top-left panel shows the results for $\rho = \rho_{\mathrm{DM}}$, the top-right panel assumes $\rho = 0.5\rho_{\mathrm{DM}}$, and the bottom panel displays the results for $\rho = 0.3\rho_{\mathrm{DM}}$. We compare results for the *correlated*, *pulsar-correlated*, and *uncorrelated* scenarios in solid, dashed, and dotted lines, respectively. Whenever the bound is prior dominated, the upper limits represent the upper end of our prior. We notice that the *pulsar-correlated* case yields valid bounds almost only when the scalar field density is $\rho = \rho_{\mathrm{DM}}$, while it is completely unconstraining when $\rho = 0.3\rho_{\mathrm{DM}}$. Priors on the parameters relevant for the search are chosen according to the scheme presented in Table I.

Therefore, the angular momentum sensitivity defined in Eq. (11) becomes

$$s_I = \frac{1}{2\beta\phi} \frac{\mathrm{d}\ln\Omega_{\mathrm{obs}}}{\mathrm{d}\phi}\bigg|_{N,J}. \tag{22}$$

Here, we cannot neglect the dependence of s_I on β; therefore, we write explicitly $s_I = s_I(\beta, M)$ or $s_I = s_I(\beta)$, depending on the context. The induced timing residual then reads

$$
\begin{aligned}
\Delta t(t) &= -\int \frac{\delta\Omega_{\mathrm{obs}}}{\bar{\Omega}} dt \\
&= -2\beta s_I(\beta) \int \frac{\rho}{m^2 M_{\mathrm{P}}^2} \hat{\phi}^2(\boldsymbol{x})\cos^2\big(mt + \theta(\boldsymbol{x})\big) \\
&= \frac{\Psi}{2m}\beta s_I(\beta)\hat{\phi}^2(\boldsymbol{x})\sin\big(2mt + \theta(\boldsymbol{x})\big)\bigg|_{t_{\mathrm{start}}}^{t_{\mathrm{end}}}, \tag{23}
\end{aligned}
$$

where we use $\Psi = \rho/(m^2 M_{\mathrm{P}}^2)$ and again neglect the dependence on the retarded time as well as the constant term in the cosine expansion, as it yields a linear contribution which is absorbed by the pulsar timing model [101–103]. As $s_I = s_I(\beta)$, Eq. (23) depends *separately* on the scalar field

density, parametrized in terms of Ψ, and on the DEF scalar coupling β. Therefore, unlike the FJBD case, ρ and β (or, equivalently, Ψ and β) must be two independent parameters of the search.

This is a crucial observation: in the FJBD case, we constrained a combination of ρ and α—namely, Ψ—and we rephrased the results into bounds on α *a posteriori*, choosing a reference value of ρ only in postprocessing. Here, instead, we are forced to impose an explicit prior on ρ. Therefore, we focus on two reference values for the scalar field density—namely, $\rho = 0.5\rho_{DM}$ and $\rho = \rho_{DM}$. Moreover, the deterministic residual in Eq. (23) depends on the sign of β, and not only on its absolute value. While one might naively think that a sign flip $\beta \to -\beta$ could be absorbed by a redefinition of the random phase $\theta(\boldsymbol{x})$, the sensitivity s_I does actually depend on the sign of β, as shown in Ref. [67] (see, e.g., Figs. 5 and 6 of that work). Hence, in the following, we present results for both positive and negative values of β. As for negative β, values $\beta \lesssim -4.3$ would generate nonperturbative strong-field effects inducing $\mathcal{O}(1)$ variations from GR [52] and are therefore not considered in the present work (being ruled out by binary pulsars [73]). Figure 3 displays the upper bounds on $|\beta|$ for the *correlated, pulsar-correlated*, and *uncorrelated* limits and for the selected MPA1 EOS, showing that our analysis implies $|\beta| \lesssim 2.2$ in the range 10^{-24} eV $\lesssim m \lesssim 10^{-23.5}$ eV for $\rho = \rho_{DM}$. We also plot the constraints obtained for a scalar field constituting 50% or 30% of DM in Fig. 3. Whenever our analysis is prior dominated, the upper limits represent the upper end (in absolute value) of our prior—namely, $|\beta| = 4.3$. As expected from the form of the signal in Eq. (23), larger values of the scalar field density yield stronger (and wider) constraints. For positive β, instead, we focus on $\beta < 150$, as the code provided in Ref. [67] to compute the sensitivities is unstable for higher values of β. The results are presented in Fig. 4 for the same choices of scalar field density. Even in this case, larger values of the scalar field density translate into more constraining upper bounds, which can be as low as $\beta \lesssim 20$ for $\rho = \rho_{DM}$. Again, the upper bounds are chosen to coincide with the upper end of our prior—namely, $\beta = 150$—whenever our analysis is prior dominated. Finally, let us recall that the analysis in Ref. [40] excludes ultralight scalar field densities $\rho \gtrsim 0.3\rho_{DM}$ for masses 10^{-24} eV $\lesssim m \lesssim 10^{-23.7}$ eV and $\rho \gtrsim 0.7\rho_{DM}$ in the mass range $10^{-23.7}$ eV $\lesssim m \lesssim 10^{-23.4}$ eV. This remark should be taken into account when interpreting the results in Figs. 3 and 4.

V. CONCLUSIONS

Conformally coupled ULDM induces periodic variations in the gravitational mass and in the radius of pulsars [67], with a timescale given by the mass of the particle. By the conservation of angular momentum, this translates into an oscillating behavior of the pulsar spin frequency, which is accurately measured by the PTA Collaborations. This effect can be used to set constraints on the coupling of ULDM to

matter, characterized by the conformal factor $\mathcal{A}(\phi)$ linking the Einstein and Jordan frame metrics. In this work, we have analyzed the FJBD and the DEF scalar-tensor theories with an ultralight scalar mass, under the assumption that the scalar field constitutes (part of) the DM, thus exploiting different functional forms of the conformal factor $\mathcal{A}(\phi)$.

In the FJBD theory, where $\mathcal{A}(\phi) \sim 1 + \alpha\phi$, we find $\log_{10} \alpha \lesssim -4.5$ across the entire frequency range considered, vastly overperforming both Cassini bounds [69] and the constraints from the pulsar in a triple stellar system [62–64]. Moreover, for masses $m \sim 10^{-23}$ eV, our analysis yields the even tighter bound, $\log_{10} \alpha \lesssim -7$. Let us recall, however, that the previously mentioned bounds have a wider range of applicability than ours, since they also constrain massless scalar-tensor theories.

In the DEF theory, where $\mathcal{A} \simeq 1 + \beta\phi^2$, we distinguish between positive and negative values of β, which yield a different expression for the sensitivity s_I. In the low-mass range, we find $-2 \lesssim \beta \lesssim 20$ for a scalar field density $\rho = \rho_{DM}$. We also explore how this bound relaxes when the scalar field density constitutes 50% or 30% of the DM density ρ_{DM}. Once again, this is competitive with respect to existing bounds that can be found in the literature [73,106,107].

In summary, we have shown that PTA data alone can constrain conformal ULDM couplings for masses below $\sim 10^{-21}$ eV at levels not yet explored by other observations. These models include scenarios where the ULDM constitutes all the dark matter in the Universe, and scenarios where the ULDM is a fraction of the total dark matter content. All the future improvements of PTA searches (e.g., those related to SKA [108]) will impact the searches we performed in this work. Furthermore, it was recently emphasized in [109] that the effects coming from the interference of the different modes comprising the ULDM field [recall Eq. (6) and the velocity dispersion $\sigma_\phi \sim 10^{-3}$] will generate a signal at frequencies below $m\sigma_\phi$ that may allow our current analysis to access ULDM models of higher masses.

APPENDIX: PARAMETERS OF THE SEARCH

Table I summarizes the parameters used in the search along with their priors. We add the label F if the parameter

TABLE I. Parameters employed for the search along with their respective priors. In the correlated limit, the parameter $\hat{\phi}_P^2$ is accounted for by a redefinition of Ψ, while in the pulsar-correlated regime $\hat{\phi}_P^2 = \hat{\phi}^2$ is a common free parameter. Only the pulsars whose masses have been measured from other experiments are presented, along with the relevant reference. For the other pulsars, we choose uniform priors with support $[M_{min}, M_{max}]$ (see main text for more details). We display the priors on the DEF scalar coupling β both for $\beta < 0$ and $\beta > 0$. $\mathcal{U}$ stands for the uniform distribution, and $\mathcal{N}$ stands for the TruncNorm distribution (see main text). The white noise parameters EFAC (TOA error Excess FACtor) and EQUAD (TOA Error excess in QUADrature) are introduced for every receiver-back-end system in every pulsar.

| Parameter	Description	Prior	Occurrence
	White noise ($\sigma = E_f^2 \sigma_{TOA}^2 + E_q^2$)		
E_f	EFAC	$\mathcal{U}(0, 10)$	1 per pulsar
E_q	EQUAD	$Log_{10} - \mathcal{U}(-10, -5)$	1 per pulsar
	Red noise (RN)		
A_{red}	RN power-law amplitude	$Log_{10} - \mathcal{U}(-20, -11)$	1 per pulsar
γ_{red}	RN power-law spectral index	$\mathcal{U}(0, 10)$	1 per pulsar
	ULDM (F)		
Ψ	ULDM signal amplitude	$Log_{10} - \mathcal{U}(-20, -12)$	1 per PTA
m [eV]	ULDM mass	$Log_{10} - \mathcal{U}(-24, -21)$	1 per PTA
$\hat{\phi}^2$	Pulsar factor	e^{-x}	1 per pulsar
θ	Pulsar signal phase	$\mathcal{U}(0, 2\pi)$	1 per pulsar
	ULDM (D)		
f_{DM}	ULDM fraction	$\mathcal{U}(0.01, 0.30)$	1 per PTA
β	DEF scalar coupling	$\mathcal{U}(-4.3, 0)$ or $\mathcal{U}(0, 150)$	1 per PTA
m [eV]	ULDM mass	$Log_{10} - \mathcal{U}(-24, -21)$	1 per PTA
$\hat{\phi}^2$	Pulsar factor	e^{-x}	1 per pulsar
θ	Pulsar signal phase	$\mathcal{U}(0, 2\pi)$	1 per pulsar
	Common spatially Uncorrelated Red Noise (CURN)		
A_{GWB}	CURN strain amplitude	$Log_{10} - \mathcal{U}(-18, -11)$	1 per PTA
γ_{GWB}	CURN spectral index	$\mathcal{U}(0, 7)$	1 per PTA
	Pulsar Masses		
M_{J0030} [113]	PSR J0030 + 0451 mass	$\mathcal{N}(1.44, 0.15)$	1 per PTA
M_{J1012} [114]	PSR J1012 + 5307 mass	$\mathcal{N}(1.72, 0.16)$	1 per PTA
M_{J1713} [115]	PSR J1713 + 0747 mass	$\mathcal{N}(1.3, 0.2)$	1 per PTA
M_{J1738} [116]	PSR J1738 + 0333 mass	$\mathcal{N}(1.47, 0.07)$	1 per PTA
M_{J1909} [117]	PSR J1909-3744 mass	$\mathcal{N}(1.438, 0.024)$	1 per PTA
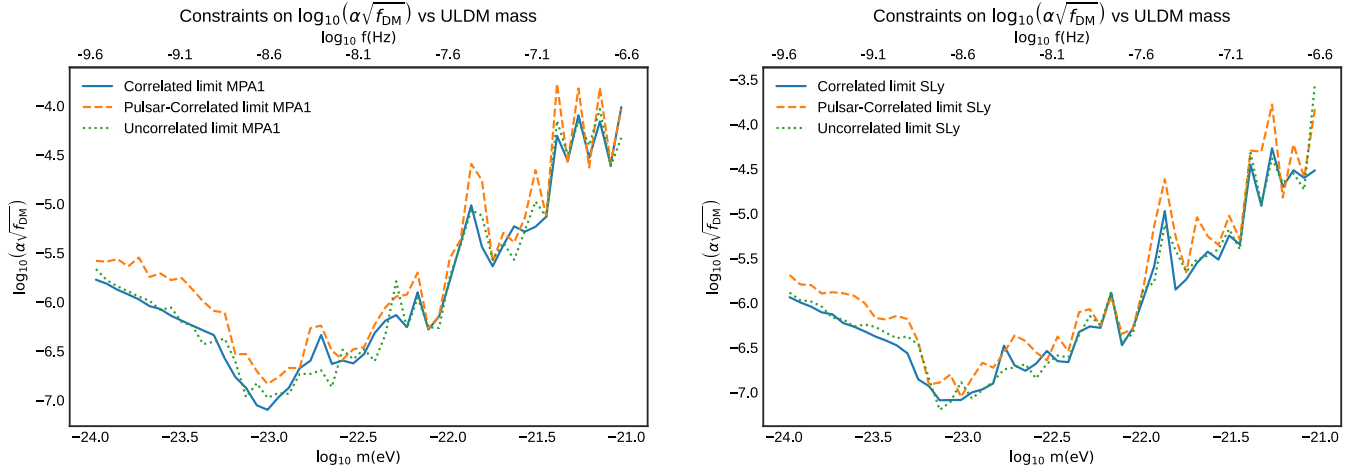
FIG. 5.   Upper limits on $\log_{10} \alpha$ at 95% credibility versus the ULDM mass, using the prescription for ρ_{DM} detailed in the main text. We compare results for the *correlated, pulsar-correlated* and *uncorrelated* scenarios in solid, dashed and dotted lines, respectively. The results are obtained using the MPA1 (left panel) and the SLy (right panel) EoS, while the priors on the parameters of the search are chosen according to Table I.

is used only in the FJBD analysis, while the label D signals parameters used only in the DEF analysis. As stated in the main text, if a pulsar mass is measured from other experiments to be $M \pm \delta M$, we sample the mass parameter from a normal prior distribution centered on M, with uncertainty δM and truncated below $M_{\min} = 1.1 M_\odot$ and above $M_{\max} = (2.2 M_\odot, 2.4 M_\odot, 2.2 M_\odot)$ for the

(AP4 [110], MPA1 [111], and SLy [112]) EoSs, respectively. We label this TruncNorm(μ, σ), where $\mu = M$ and $\sigma = \delta M$. Otherwise, we just assume a uniform prior between $M_{\min}$ and $M_{\max}$ for the three EoS choices. We also plot in Fig. 5 the constraints on the FJBD scalar coupling α for the different EoSs of the pulsar interior presented in Ref. [67].

[1] Ricardo A. Flores and Joel R. Primack, Observational and theoretical constraints on singular dark matter halos, Astrophys. J. Lett. **427,** L1 (1994).

[2] Ben Moore, Evidence against dissipation-less dark matter from observations of galaxy haloes, Nature (London) **370,** 629 (1994).

[3] E. V. Karukes, P. Salucci, and G. Gentile, The dark matter distribution in the spiral NGC 3198 out to 0.22 R$_{vir}$, Astron. Astrophys. **578,** A13 (2015).

[4] Anatoly Klypin, Andrey V. Kravtsov, Octavio Valenzuela, and Francisco Prada, Where are the missing galactic satellites?, Astrophys. J. **522,** 82 (1999).

[5] Ben Moore, Sebastiano Ghigna, Fabio Governato, George Lake, Thomas Quinn, Joachim Stadel, and Paolo Tozzi, Dark matter substructure within galactic halos, Astrophys. J. Lett. **524,** L19 (1999).

[6] Michael Boylan-Kolchin, James S. Bullock, and Manoj Kaplinghat, Too big to fail? The puzzling darkness of massive Milky Way subhaloes, Mon. Not. R. Astron. Soc. **415,** L40 (2011).

[7] J. F. Navarro, V. R. Eke, and C. S. Frenk, The cores of dwarf galaxy haloes, Mon. Not. R. Astron. Soc. **283,** L72 (1996).

[8] F. Governato, A. Zolotov, A. Pontzen, C. Christensen, S. H. Oh, A. M. Brooks, T. Quinn, S. Shen, and J. Wadsley, Cuspy no more: How outflows affect the central dark matter and baryon distribution in Λ cold dark matter galaxies, Mon. Not. R. Astron. Soc. **422,** 1231 (2012).

[9] Alyson M. Brooks, Michael Kuhlen, Adi Zolotov, and Dan Hooper, A baryonic solution to the missing satellites problem, Astrophys. J. **765,** 22 (2013).

[10] T. K. Chan, D. Kereš, J. Oñorbe, P. F. Hopkins, A. L. Muratov, C.-A. Faucher-Giguère, and E. Quataert, The impact of baryonic physics on the structure of dark matter haloes: The view from the FIRE cosmological simulations, Mon. Not. R. Astron. Soc. **454,** 2981 (2015).

[11] Jose Oñorbe, Michael Boylan-Kolchin, James S. Bullock, Philip F. Hopkins, Dušan Kereš, Claude-André Faucher-Giguère, Eliot Quataert, and Norman Murray, Forged in fire: Cusps, cores and baryons in low-mass dwarf galaxies, Mon. Not. R. Astron. Soc. **454,** 2092 (2015).

[12] J. I. Read, O. Agertz, and M. L. M. Collins, Dark matter cores all the way down, Mon. Not. R. Astron. Soc. **459,** 2573 (2016).

[13] Wayne Hu, Rennan Barkana, and Andrei Gruzinov, Cold and fuzzy dark matter, Phys. Rev. Lett. **85,** 1158 (2000).

[14] Lam Hui, Jeremiah P. Ostriker, Scott Tremaine, and Edward Witten, Ultralight scalars as cosmological dark matter, Phys. Rev. D **95**, 043541 (2017).

[15] Michael B. Green, J. H. Schwarz, and Edward Witten, *Superstring Theory, Vol. 1: Introduction*, Cambridge Monographs on Mathematical Physics (Cambridge University Press, Cambridge, England, 1988).

[16] Peter Svrcek and Edward Witten, Axions in string theory, J. High Energy Phys. 06 (2006) 051.

[17] Asimina Arvanitaki, Savas Dimopoulos, Sergei Dubovsky, Nemanja Kaloper, and John March-Russell, String axiverse, Phys. Rev. D **81**, 123530 (2010).

[18] Renée Hlozek, Daniel Grin, David J. E. Marsh, and Pedro G. Ferreira, A search for ultralight axions using precision cosmological data, Phys. Rev. D **91**, 103512 (2015).

[19] Vid Iršič, Matteo Viel, Martin G. Haehnelt, James S. Bolton, and George D. Becker, First constraints on fuzzy dark matter from Lyman-α forest data and hydrodynamical simulations, Phys. Rev. Lett. **119**, 031302 (2017).

[20] Eric Armengaud, Nathalie Palanque-Delabrouille, Christophe Yèche, David J. E. Marsh, and Julien Baur, Constraining the mass of light bosonic dark matter using SDSS Lyman-α forest, Mon. Not. R. Astron. Soc. **471**, 4606 (2017).

[21] Takeshi Kobayashi, Riccardo Murgia, Andrea De Simone, Vid Iršič, and Matteo Viel, Lyman-α constraints on ultralight scalar dark matter: Implications for the early and late Universe, Phys. Rev. D **96**, 123514 (2017).

[22] Matteo Nori, Riccardo Murgia, Vid Iršič, Marco Baldi, and Matteo Viel, Lyman-α forest and non-linear structure characterization in fuzzy dark matter cosmologies, Mon. Not. R. Astron. Soc. **482**, 3227 (2018).

[23] Keir K. Rogers and Hiranya V. Peiris, Strong bound on canonical ultralight axion dark matter from the Lyman-α forest, Phys. Rev. Lett. **126**, 071302 (2021).

[24] Hsi-Yu Schive, Ming-Hsuan Liao, Tak-Pong Woo, Shing-Kwong Wong, Tzihong Chiueh, Tom Broadhurst, and W.-Y. Pauchy Hwang, Understanding the core-halo relation of quantum wave dark matter from 3D simulations, Phys. Rev. Lett. **113**, 261302 (2014).

[25] Jiajun Zhang, Hantao Liu, and Ming-Chung Chu, Cosmological simulation for fuzzy dark matter model, Front. Astron. Space Sci. (2019), 10.3389/fspas.2018.00048.

[26] Nitsan Bar, Diego Blas, Kfir Blum, and Sergey Sibiryakov, Galactic rotation curves versus ultralight dark matter: Implications of the soliton-host halo relation, Phys. Rev. D **98**, 083027 (2018).

[27] Kohei Hayashi, Elisa G. M. Ferreira, and Hei Yin Jowett Chan, Narrowing the mass range of fuzzy dark matter with ultrafaint dwarfs, Astrophys. J. Lett. **912**, L3 (2021).

[28] Neal Dalal and Andrey Kravtsov, Excluding FDM with sizes and stellar kinematics of ultra-faint dwarf galaxies, Phys. Rev. D **106**, 063517 (2022).

[29] David J. E. Marsh and Jens C. Niemeyer, Strong constraints on fuzzy dark matter from ultrafaint dwarf galaxy Eridanus II, Phys. Rev. Lett. **123**, 051103 (2019).

[30] Elisa G. M. Ferreira, Ultra-light dark matter, Astron. Astrophys. Rev. **29**, 7 (2021).

[31] Asimina Arvanitaki, Savas Dimopoulos, Sergei Dubovsky, Nemanja Kaloper, and John March-Russell, String axiverse, Phys. Rev. D **81**, 123530 (2010).

[32] Louis Hamaide, Hendrik Müller, and David J. E. Marsh, Searching for dilaton fields in the Lyman-α forest, Phys. Rev. D **106**, 123509 (2022).

[33] Andrei Khmelnitsky and Valery Rubakov, Pulsar timing signal from ultralight scalar dark matter, J. Cosmol. Astropart. Phys. 02 (2014) 019.

[34] R. S. Foster and D. C. Backer, Constructing a pulsar timing array, Astrophys. J. **361**, 300 (1990).

[35] R. N. Manchester *et al.*, The Parkes Pulsar Timing Array project, Publ. Astron. Soc. Aust. **30**, e017 (2013).

[36] M. A. McLaughlin, The North American nanohertz observatory for gravitational waves, Classical Quantum Gravity **30**, 224008 (2013).

[37] Michael Kramer and David J. Champion, The European Pulsar Timing Array and the Large European Array for Pulsars, Classical Quantum Gravity **30**, 224009 (2013).

[38] Bhal Chandra Joshi *et al.*, Precision pulsar timing with the ORT and the GMRT and its applications in pulsar astrophysics, J. Astrophys. Astron. **39**, 51 (2018).

[39] M. Bailes *et al.*, The MeerKAT telescope as a pulsar facility: System verification and early science results from MeerTime, Publ. Astron. Soc. Aust. **37**, e028 (2020).

[40] Clemente Smarra *et al.* (EPTA Collaboration), Second data release from the European Pulsar Timing Array: Challenging the ultralight dark matter paradigm, Phys. Rev. Lett. **131**, 171001 (2023).

[41] Nataliya K. Porayko *et al.*, Parkes Pulsar Timing Array constraints on ultralight scalar-field dark matter, Phys. Rev. D **98**, 102002 (2018).

[42] David E. Kaplan, Andrea Mitridate, and Tanner Trickle, Constraining fundamental constant variations from ultralight dark matter with pulsar timing arrays, Phys. Rev. D **106**, 035032 (2022).

[43] Adeela Afzal *et al.* (The NANOGrav Collaboration), The NANOGrav 15 yr data set: Search for signals from new physics, Astrophys. J. Lett. **951**, L11 (2023).

[44] Diego Blas, Diana López Nacir, and Sergey Sibiryakov, Ultralight dark matter resonates with binary pulsars, Phys. Rev. Lett. **118**, 261102 (2017).

[45] Diego Blas, Diana López Nacir, and Sergey Sibiryakov, Secular effects of ultralight dark matter on binary pulsars, Phys. Rev. D **101**, 063016 (2020).

[46] Pavel Kůs, Diana López Nacir, and Federico R. Urban, Bayesian sensitivity of binary pulsars to ultra-light dark matter, arXiv:2402.04099.

[47] M. Fierz, On the physical interpretation of P. Jordan's extended theory of gravitation, Helv. Phys. Acta **29**, 128 (1956).

[48] Pascual Jordan, The present state of Dirac's cosmological hypothesis, Z. Phys. **157**, 112 (1959).

[49] C. Brans and R. H. Dicke, Mach's principle and a relativistic theory of gravitation, Phys. Rev. **124**, 925 (1961).

[50] R. H. Dicke, Mach's principle and invariance under transformation of units, Phys. Rev. **125**, 2163 (1962).

[51] Thibault Damour and Gilles Esposito-Farese, Tensor multiscalar theories of gravitation, Classical Quantum Gravity **9**, 2093 (1992).

[52] Thibault Damour and Gilles Esposito-Farèse, Nonperturbative strong-field effects in tensor-scalar theories of gravitation, Phys. Rev. Lett. **70**, 2220 (1993).

[53] Justin Alsing, Emanuele Berti, Clifford M. Will, and Helmut Zaglauer, Gravitational radiation from compact binary systems in the massive Brans-Dicke theory of gravity, Phys. Rev. D **85**, 064041 (2012).

[54] Kenneth Nordtvedt, Equivalence principle for massive bodies: II. Theory, Phys. Rev. **169**, 1017 (1968).

[55] D. M. Eardley, Observable effects of a scalar gravitational field in a binary pulsar, Astrophys. J. **196**, L59 (1975).

[56] Clifford M. Will and Helmut W. Zaglauer, Gravitational radiation, close binary systems, and the Brans-Dicke theory of gravity, Astrophys. J. **346**, 366 (1989).

[57] C. M. Will, Gravitational radiation from binary systems in alternative metric theories of gravity: Dipole radiation and the binary pulsar, Astrophys. J. **214**, 826 (1977).

[58] C. M. Will, *Theory and Experiment in Gravitational Physics* (Cambridge University Press, 1993).

[59] Thibault Damour and Joseph H. Taylor, Strong field tests of relativistic gravity and binary pulsars, Phys. Rev. D **45**, 1840 (1992).

[60] J. M. Weisberg and J. H. Taylor, Relativistic binary pulsar B1913 + 16: Thirty years of observations and analysis, arXiv:astro-ph/0407149.

[61] M. Kramer, Ingrid H. Stairs, R. N. Manchester, M. A. McLaughlin, A. G. Lyne *et al.*, Tests of general relativity from timing the double pulsar, Science **314**, 97 (2006).

[62] S. M. Ransom *et al.*, A millisecond pulsar in a stellar triple system, Nature (London) **505**, 520 (2014).

[63] Anne M. Archibald, Nina V. Gusinskaia, Jason W. T. Hessels, Adam T. Deller, David L. Kaplan, Duncan R. Lorimer, Ryan S. Lynch, Scott M. Ransom, and Ingrid H. Stairs, Universality of free fall from the orbital motion of a pulsar in a stellar triple system, Nature (London) **559**, 73 (2018).

[64] G. Voisin, I. Cognard, P. C. C. Freire, N. Wex, L. Guillemot, G. Desvignes, M. Kramer, and G. Theureau, An improved test of the strong equivalence principle with the pulsar in a triple star system, Astron. Astrophys. **638**, A24 (2020).

[65] M. Kramer *et al.*, Strong-field gravity tests with the double pulsar, Phys. Rev. X **11**, 041050 (2021).

[66] Junjie Zhao, Paulo C. C. Freire, Michael Kramer, Lijing Shao, and Norbert Wex, Closing a spontaneous-scalarization window with binary pulsars, Classical Quantum Gravity **39**, 11LT01 (2022).

[67] Adrien Kuntz and Enrico Barausse, Angular momentum sensitivities in scalar-tensor theories, Phys. Rev. D **109**, 124001 (2024).

[68] Thibault Damour and Gilles Esposito-Farèse, Tensor-scalar gravity and binary-pulsar experiments, Phys. Rev. D **54**, 1474 (1996).

[69] B. Bertotti, L. Iess, and P. Tortora, A test of general relativity using radio links with the Cassini spacecraft, Nature (London) **425**, 374 (2003).

[70] T. Damour and Alexander M. Polyakov, The string dilaton and a least coupling principle, Nucl. Phys. **B423**, 532 (1994).

[71] Jihn E. Kim, Light pseudoscalars, particle physics and cosmology, Phys. Rep. **150**, 1 (1987).

[72] Clifford M. Will, *Theory and Experiment in Gravitational Physics* (Cambridge University Press, Cambridge, England, 1993).

[73] Lijing Shao, Noah Sennett, Alessandra Buonanno, Michael Kramer, and Norbert Wex, Constraining nonperturbative strong-field effects in scalar-tensor gravity by combining pulsar timing and laser-interferometer gravitational-wave detectors, Phys. Rev. X **7**, 041025 (2017).

[74] Andrés Castillo, Jorge Martin-Camalich, Jorge Terol-Calvo, Diego Blas, Andrea Caputo, Ricardo Tanausú Génova Santos, Laura Sberna, Michael Peel, and Jose Alberto Rubiño Martín, Searching for dark-matter waves with PPTA and QUIJOTE pulsar polarimetry, J. Cosmol. Astropart. Phys. 06 (2022) 014.

[75] Fabrizio Nesti and Paolo Salucci, The dark matter halo of the Milky Way, AD 2013, J. Cosmol. Astropart. Phys. 07 (2013) 016.

[76] J. Antoniadis *et al.* (EPTA Collaboration), The second data release from the European Pulsar Timing Array: I. The dataset and timing analysis, Astron. Astrophys. **678**, A48 (2023).

[77] G. Desvignes *et al.*, High-precision timing of 42 millisecond pulsars with the European Pulsar Timing Array, Mon. Not. R. Astron. Soc. **458**, 3341 (2016).

[78] R. T. Edwards, G. B. Hobbs, and R. N. Manchester, TEMPO2, a new pulsar timing package: II. The timing model and precision estimates, Mon. Not. R. Astron. Soc. **372**, 1549 (2006).

[79] Boris Goncharov, D. J. Reardon, R. M. Shannon, Xing-Jiang Zhu, Eric Thrane, M. Bailes, N. D. R. Bhat, S. Dai, G. Hobbs, M. Kerr, R. N. Manchester, S. Osłowski, A. Parthasarathy, C. J. Russell, R. Spiewak, N. Thyagarajan, and J. B. Wang, Identifying and mitigating noise sources in precision pulsar timing data sets, Mon. Not. R. Astron. Soc. **502**, 478 (2021).

[80] J. Antoniadis *et al.* (EPTA and InPTA Collaborations), The second data release from the European Pulsar Timing Array: II. Customised pulsar noise models for spatially correlated gravitational waves, Astron. Astrophys. **678**, A49 (2023).

[81] Gabriella Agazie *et al.* (NANOGrav Collaboration), The NANOGrav 15 yr data set: Evidence for a gravitational-wave background, Astrophys. J. Lett. **951**, L8 (2023).

[82] J. Antoniadis *et al.* (EPTA, InPTA Collaborations), The second data release from the European Pulsar Timing Array: III. Search for gravitational wave signals, Astron. Astrophys. **678**, A50 (2023).

[83] Daniel J. Reardon *et al.*, Search for an isotropic gravitational-wave background with the Parkes Pulsar Timing Array, Astrophys. J. Lett. **951**, L6 (2023).

[84] Heng Xu *et al.*, Searching for the nano-hertz stochastic gravitational wave background with the Chinese Pulsar Timing Array Data Release I, Res. Astron. Astrophys. **23**, 075024 (2023).

[85] R. W. Hellings and G. S. Downs, Upper limits on the isotropic gravitational radiation background from pulsar timing analysis, Astrophys. J. Lett. **265**, L39 (1983).

[86] J. Antoniadis *et al.* (EPTA and InPTA Collaborations), The second data release from the European Pulsar Timing Array: III. Search for gravitational wave signals, Astron. Astrophys. **678**, A50 (2023).

[87] J. Antoniadis *et al.*, The second data release from the European Pulsar Timing Array: V. Implications for massive black holes, dark matter and the early Universe, Astron. Astrophys. **685**, A94 (2024).

[88] Zaven Arzoumanian *et al.* (Nanograv Collaboration), The NANOGrav 12.5 yr data set: Search for an isotropic stochastic gravitational-wave background, Astrophys. J. Lett. **905**, L34 (2020).

[89] Boris Goncharov *et al.*, On the evidence for a common-spectrum process in the search for the nanohertz gravitational-wave background with the Parkes Pulsar Timing Array, Astrophys. J. Lett. **917**, L19 (2021).

[90] S. Chen *et al.*, Common-red-signal analysis with 24-yr high-precision timing of the European Pulsar Timing Array: Inferences in the stochastic gravitational-wave background search, Mon. Not. R. Astron. Soc. **508**, 4970 (2021).

[91] Rutger van Haasteren, Yuri Levin, Patrick McDonald, and Tingting Lu, On measuring the gravitational-wave background using Pulsar Timing Arrays, Mon. Not. R. Astron. Soc. **395**, 1005 (2009).

[92] L. Lentati, P. Alexander, M. P. Hobson, F. Feroz, R. van Haasteren, K. J. Lee, and R. M. Shannon, TEMPONEST: A Bayesian approach to pulsar timing analysis, Mon. Not. R. Astron. Soc. **437**, 3004 (2014).

[93] S. R. Taylor, L. Lentati, S. Babak, P. Brem, J. R. Gair, A. Sesana, and A. Vecchio, All correlations must die: Assessing the significance of a stochastic gravitational-wave background in Pulsar Timing Arrays, Phys. Rev. D **95**, 042002 (2017).

[94] Justin A. Ellis, Michele Vallisneri, Stephen R. Taylor, and Paul T. Baker, ENTERPRISE: Enhanced numerical toolbox enabling a robust pulsar inference suite, Zenodo (2020).

[95] Stephen R. Taylor, Paul T. Baker, Jeffrey S. Hazboun, Joseph Simon, and Sarah J. Vigeland, ENTERPRISE_EXTENSIONS v2.3.3 (2021).

[96] Justin Ellis and Rutger van Haasteren, jellis18/ptmcmcsampler: Official release (2017).

[97] Andrea Mitridate, PTArcade, 10.5281/zenodo.7876430 (2023).

[98] Andrea Mitridate, David Wright, Richard von Eckardstein, Tobias Schröder, Jonathan Nay, Ken Olum, Kai Schmitz, and Tanner Trickle, PTArcade, arXiv:2306.16377.

[99] J. P. W. Verbiest, J. M. Weisberg, A. A. Chael, K. J. Lee, and D. R. Lorimer, On pulsar distance measurements and their uncertainties, Astrophys. J. **755**, 39 (2012).

[100] Jai chan Hwang, Donghui Jeong, Hyerim Noh, and Clemente Smarra, Pulsar timing array signature from oscillating metric perturbations due to ultra-light axion, J. Cosmol. Astropart. Phys. 02 (2024) 014.

[101] Jeffrey S. Hazboun, Joseph D. Romano, and Tristan L. Smith, Realistic sensitivity curves for pulsar timing arrays, Phys. Rev. D **100**, 104028 (2019).

[102] R. Blandford, R. Narayan, and R. W. Romani, Arrival-time analysis for a millisecond pulsar, J. Astrophys. Astron. **5**, 369 (1984).

[103] Harikrishnan Ramani, Tanner Trickle, and Kathryn M. Zurek, Observability of dark matter substructure with pulsar timing correlations, J. Cosmol. Astropart. Phys. 12 (2020) 033.

[104] Caner Unal, Federico R. Urban, and Ely D. Kovetz, Probing ultralight scalar, vector and tensor dark matter with pulsar timing arrays, arXiv:2209.02741.

[105] Mark Abney, Richard I. Epstein, and Angela V. Olinto, Observational constraints on the internal structure and dynamics of the Vela Pulsar, Astrophys. J. **466**, L91 (1996).

[106] Raissa F. P. Mendes, Possibility of setting a new constraint to scalar-tensor theories, Phys. Rev. D **91**, 064024 (2015).

[107] David Anderson and Nicolás Yunes, Solar System constraints on massless scalar-tensor gravity with positive coupling constant upon cosmological evolution of the scalar field, Phys. Rev. D **96**, 064037 (2017).

[108] Gemma Janssen *et al.*, Gravitational wave astronomy with the SKA, Proc. Sci. AASKA14 (**2015**) 037 [arXiv:1501.00127].

[109] Hyungjin Kim, Gravitational interaction of ultralight dark matter with interferometers, J. Cosmol. Astropart. Phys. 12 (2023) 018.

[110] A. Akmal, V. R. Pandharipande, and D. G. Ravenhall, Equation of state of nucleon matter and neutron star structure, Phys. Rev. C **58**, 1804 (1998).

[111] H. Müther, M. Prakash, and T. L. Ainsworth, The nuclear symmetry energy in relativistic Brueckner-Hartree-Fock calculations, Phys. Lett. B **199**, 469 (1987).

[112] F. Douchin and P. Haensel, A unified equation of state of dense matter and neutron star structure, Astron. Astrophys. **380**, 151 (2001).

[113] M. C. Miller *et al.*, PSR J0030 + 0451 mass and radius from nicer data and implications for the properties of neutron star matter, Astrophys. J. Lett. **887**, L24 (2019).

[114] D. Mata Sánchez, A. G. Istrate, M. H. van Kerkwijk, R. P. Breton, and D. L. Kaplan, PSR J1012 + 5307: A millisecond pulsar with an extremely low-mass white dwarf companion, Mon. Not. R. Astron. Soc. **494**, 4031 (2020).

[115] W.-C. Chen and J. A. Panei, The progenitor of binary millisecond radio pulsar PSR J1713 + 0747, Astron. Astrophys. **527**, A128 (2011).

[116] J. Antoniadis, M. H. van Kerkwijk, D. Koester, P. C. C. Freire, N. Wex, T. M. Tauris, M. Kramer, and C. G. Bassa, The relativistic pulsar–white dwarf binary PSR J1738 + 0333: I. Mass determination and evolutionary history, Mon. Not. R. Astron. Soc. **423**, 3316 (2012).

[117] B. A. Jacoby, A. Hotan, M. Bailes, S. Ord, and S. R. Kulkarni, The mass of a millisecond pulsar, Astrophys. J. **629**, L113 (2005).